ACS OMEGA

http://pubs.acs.org/journal/acsodf

Article

Metal-Free Homocoupling of Pyrene inside the Pores of Mesoporous Carbons via Electrochemical Oxidation: Application for Electrochemical Capacitors

Hiroyuki Itoi,* Kazuki Takagi, Hayato Ohmi, Takanori Usami, Yuto Nagai, Chika Matsuoka, Ryutaro Suzuki, Shinichi Kugimiya, Hiroyuki Iwata, and Yoshimi Ohzawa

Cite This: *ACS Omega* 2022, 7, 35245−35255

Read Online

ACCESS | Metrics & More | Article Recommendations | Supporting Information

ABSTRACT: A pyrene dimer (PYD) is synthesized by electrochemical oxidation *via* homocoupling of pyrene (PY) inside the pores of MgO-templated mesoporous carbons without any metal catalysts or organic solvents. The resulting MgO-C/PYD hybrids can be used as high-performance aqueous electrochemical capacitor electrodes due to the reversible redox property of PYD and large contact area between the hybridized PYD and conductive carbon surfaces, which enable rapid charge transfer at the large contact interface. In our previous study, PY was considered to polymerize through electrochemical oxidation, and activated carbon with the pore sizes of ∼4 nm was used as a porous carbon substrate. In this study, the MgO-templated carbons have the average pore sizes of 5, 10, and 30 nm, and their large mesopore volumes can accommodate a large amount of PYD for enhancing the capacitance. To develop high-performance electrochemical capacitors, the dependence of the capacitance enhancement and the capacitance retention on the amount of PY and the pore sizes of MgO-templated carbons are studied. It is found that mesopores are necessary for fast charging/discharging, but the capacitance retention and capacitance enhancement decrease with increasing the mesopore sizes and the amount of PY due to the decreased utilization ratio of PY.

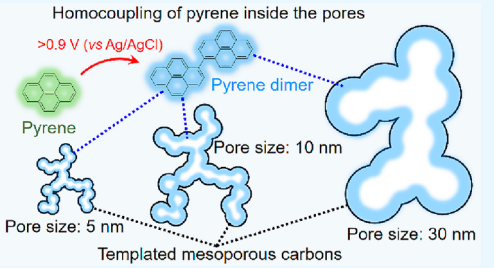

1. INTRODUCTION

Porous carbons, as represented by activated carbon (AC), are industrially mass-produced materials and have been applied to purification and separation technologies due to their strong adsorption capability and large surface area. In addition, since porous carbons have chemical stability and high electrical conductivity, they have been also used as electrode materials for electric double-layer capacitors (EDLCs)[1,2] and fuel cells.[3,4] EDLCs are electrical energy storage devices using the electric double layer (EDL) during charging and discharging.[5] The formation of the EDL is a physical process and does not involve chemical reactions. Such a physical process is regarded as proceeding more rapidly than chemical reactions and is not accompanied by the degradation of electrode materials and electrolytes.[2,6] Therefore, EDLCs have superior power densities and cycle lifetimes than those of secondary batteries such as lithium-ion batteries. However, one of the biggest drawbacks of EDLCs is their small energy densities in comparison with those of secondary batteries.

The hybrids of porous carbons and redox-active materials are categorized into electrochemical capacitors and have higher energy densities than those of EDLCs due to the high energy density characteristics of redox-active materials.[7−9] Metal oxides,[10−12] conductive polymers,[13−15] and redox-active organic compounds[16,17] are representative redox-active materials, and they are hybridized as particles, films, and fibers because most of them have poor electrical conductivities. The hybridization allows the redox-active materials with charge transfer at the contact interface between redox-active materials and conductive carbon surfaces. Therefore, the way of hybridization decides not only the energy densities of the hybrids but also their power densities. We have recently reported the hybridization of porous carbons with redox-active materials for enhancing the energy and power densities of the hybrids.[18−23] In this method, redox-active materials are hybridized inside the pores of porous carbons, and the resulting large contact areas between redox-active materials and conductive carbon surfaces enable rapid charge transfer at the contact interface. Moreover, the volumetric energy density, which is a more practical index than the gravimetric one for the application of electrical energy storage devices, can be effectively enhanced by the hybridization because the hybridization is not associated with the volume expansion of porous carbon particles. The power densities of the hybrids are higher

Received: July 18, 2022
Accepted: September 8, 2022
Published: September 21, 2022

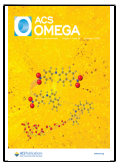

https://doi.org/10.1021/acsomega.2c04511
ACS Omega 2022, 7, 35245−35255

than those of the porous carbons that are used as EDLC electrodes. Therefore, the hybrids are used as asymmetrical electrochemical capacitor electrodes by combining with appropriate counterpart electrodes to balance the power densities of anodes and cathodes. Among the redox-active materials examined, a conductive polymer precursor, pyrene (PY), shows enhanced volumetric capacitances with retaining a high power density up to 10 A g^{-1} upon polarization within the pores of AC.[24] The AC had not only micropores but also a large fraction of mesopores with the sizes of up to 4 nm to accommodate a large amount of PY. Our subsequent concern is how much the volumetric capacitance can be enhanced with retaining a high power density by using PY and mesoporous carbons because mesoporous carbons have a large amount of a pore volume to further enhance the volumetric capacitance toward future electronic devices and others. In addition, although the redox-active properties were thought to be derived from polypyrene[25] in our previous study, the characterization of the causative redox-active materials is necessary for revealing the correlation with the electrochemical capacitor performances.

Here, we demonstrate the metal-free homocoupling of PY to a PY dimer (PYD) *via* the electrochemical oxidation of PY inside the pores of MgO-templated mesoporous carbons (MgO-Cs).[26,27] The advantages of the use of MgO to prepare mesoporous carbons lie in the chemical stability and the resistances to reduction and formation of carbides during the carbonization process to synthesize mesoporous carbons. Moreover, MgO is relatively inexpensive and industrially readily available because the resources of MgO are readily available. Furthermore, MgO is easily removed by diluted HCl, and MgO-templated carbons are therefore capable of mass production. PY is not polymerized inside the pores of porous carbons due to the pore constraint but undergoes homocoupling, irrespective of the absence of any metal catalysts or organic solvents. The homocoupling requires the conductive carbon surface and would be achieved by the pore confinement because the intermediate radical cation is unstable and intrinsically repels each other.[28] MgO-Cs have a large amount of pore volumes (~1.95 cm^3 g^{-1}) and can accommodate a large amount of PY. We discuss the effects of the amount of PY and the pore size of MgO-Cs on the volumetric capacitance enhancement and rate capability. The resulting MgO-C/PYD hybrids show an increasing volumetric capacitance up to six times higher than those of the pristine MgO-Cs with increasing PY contents. In addition, they balance high rate capability up to a high current density of 10 A g^{-1} and long cycle lifetimes.

2. EXPERIMENTAL SECTION

2.1. Synthesis. Three kinds of MgO-templated carbons (MgO-Cs; TOYO TANSO) with the average pore sizes of 5, 10, and 30 nm (CNovel MH, MJ(4)010, and MJ(4)030, respectively; TOYO TANSO) are denoted MgO-C (5), MgO-C (10), and MgO-C (30), respectively. MgO-C was dried at 150 °C (ramp rate: 5 °C min^{-1}) for 1 h under vacuum. The weight of the dried MgO-C was measured and mixed with PY (PY; FUJIFILM Wako Pure Chemical Corp.) at the MgO-C/PY weight ratios of 7:3 and 1:1; *i.e.*, the weight percentages of PY in the mixtures are 30 and 50 wt %, respectively. The mixture was introduced in a glass ampoule, and the ampoule was sealed under vacuum. Adsorption was performed at 150 °C for 24 and 48 h for 30 and 50 wt % of PY in the mixtures, respectively. The resulting MgO-C/PY samples are denoted MgO-C (X)/PY (Y), where X and Y represent the average pore size of MgO-C in nanometers and the weight percent of PY in the samples, respectively.

2.2. Measurements and Electrochemical Procedures. A nitrogen adsorption/desorption measurement was performed at −196 °C with ASAP 2020 (Micromeritics). MgO-Cs were previously dried at 150 °C for 1 h to remove the adsorbed water from MgO-C. The Brunauer−Emmett−Teller (BET) specific surface areas of the MgO-Cs were calculated using the adsorption isotherms in a P/P_0 range from 0.05 to 0.20. The total pore volume was determined from the adsorption amount of nitrogen at P/P_0 of 0.96. The micropore volume was estimated by the Dubinin−Radushkevich method, and the mesopore volume was calculated by subtracting the micropore volume from the total pore volume. Transmission electron microscopy (TEM) observation and energy-dispersive X-ray spectroscopy (EDS) analysis were performed using JEM-2100Plus (JEOL) equipped with a Noran System 7 EDL system with a scanning device comprised of bright-field (BF) and annular dark-field (ADF) detectors. The accelerating voltage was 200 kV, and a Mo grid was used for the TEM observation. Scanning electron microscopy (SEM) observation was conducted with Superscan SS-550 (Shimadzu) at an accelerating voltage of 15 kV. Electrochemical measurements were conducted at 25 °C with a three-electrode beaker cell using 1 M aqueous H_2SO_4 and Ag/AgCl (sat. KCl) reference electrode. The details of the electrode preparation and cell assembly are described in the Supporting Information.[24] Briefly, the MgO-C or MgO-C/PY sample was mixed with polytetrafluoroethylene (PTFE) and carbon black (CB) at a MgO-C/PTFE/CB weight ratio of 18:1:1 for preparing a working electrode. The resulting mixture was shaped into a 12 mm square sheet containing 8.5 mg of MgO-C and sandwiched by stainless mesh (100 mesh) under precisely controlled conditions (30 MPa, 150 s) with a Compact Table-Top Universal/Tensile Tester (EZ-LX, Shimadzu). A counter electrode was prepared by using activated carbon (AC; MSC30, Kansai Coke and Chemicals Co., Ltd.) in the same manner as that used to prepare the working electrode. To measure the electrode density, the mixture of the sample, PTFE, and CB prepared for the working electrode was pressed into the pellet with a diameter of 13 mm under the same conditions as those used for preparing the working electrode (*i.e.*, 30 MPa, 150 s). The electrode density was calculated from the weight and thickness of the pellet, which were precisely measured by microbalance (XPR2V, Mettler Toledo) and micrometer (DIGIMICRO, MF-501, Nikon), respectively. The theoretical electrode density (ρ^{theo} g cm^{-3}) was calculated from the following equation:[24]

$$\rho^{theo} = \rho^{ex}_{MgO-C}\left(\frac{90}{100 - Y} + 0.1\right)$$

where ρ^{ex}_{MgO-C} (g cm^{-3}) is the experimental electrode density of the corresponding pristine MgO-C and Y is the weight percentage of PY in the MgO-C/PY samples (*vide supra*).

Cyclic voltammetry (CV), impedance analysis, and galvanostatic charge/discharge analysis (GC) were done using the apparatuses described previously.[22] The homocoupling of PY in the MgO-C/PY samples was performed by CV at a sweep rate of 5 mV s^{-1} between −0.1 and 1.2 V (*vs* Ag/AgCl). The resulting MgO-C/pyrene dimer (PYD) hybrids are denoted MgO-C (X)/PYD (Y). Electrochemical capacitor performances of the MgO-C/PYD hybrids were first examined by CV

https://doi.org/10.1021/acsomega.2c04511
ACS Omega 2022, 7, 35245−35255

at 1 mV s^{-1} between −0.1 and 0.8 V. Subsequently, an impedance spectrum was collected at an anodic peak top potential with a potential amplitude of 10 mV in a frequency range of 10^{-2} to 10^{5} Hz. GC was conducted in a potential range of −0.1 to 0.8 V. The gravimetric capacitance (C_g F g^{-1}) was calculated according to the following equation:

$$C_g = \frac{I\Delta t}{m\Delta V}$$

where I (A) is the current, Δt (s) is the time from −0.1 to 0.8 V, m is the weight (g) of MgO-C and PY in the working electrode, and ΔV (V) is fixed to 0.9 V irrespective of the current density. The volumetric capacitance (C_V F cm^{-3}) was calculated, assuming that PYD was hybridized inside the pores of MgO-C without the volume expansion of MgO-C particles, using the following equation:[22,23]

$$C_V = \frac{90 C_g \rho^{ex}_{MgO-C}}{100 - Y}$$

The volumetric current (I_V A cm^{-3}) was calculated in a similar manner for calculating the volumetric capacitance, as shown in the following equation:

$$I_V = \frac{90 I_g \rho^{ex}_{MgO-C}}{100 - Y}$$

Matrix-assisted laser desorption ionization time-of-flight mass spectrometry (MALDI-TOF-MS) analysis was performed on an AXIMA Assurance (Shimadzu) with a nitrogen laser (337 nm) without a matrix. After the electrochemical oxidation, the MgO-C/PYD hybrid was removed from a current collector by ultrasonication in 100 mL of deionized water and further washed thoroughly with stirring at 25 °C for 24 h. The aqueous solution was filtered, and the MgO-C/PYD hybrid was dried under vacuum at room temperature overnight. The dried sample was again stirred in 4 mL of dichloromethane at 25 °C for 24 h to extract PYD. The solution was filtered and the filtrate was analyzed without any matrices or ionization reagents.

3. RESULTS AND DISCUSSION

In this study, we examined three kinds of MgO-templated carbons (MgO-Cs) with the average pore sizes of 5, 10, and 30 nm (Figure S1), which are denoted MgO-C (5), MgO-C (10), and MgO-C (30), respectively. Their Brunauer−Emmett−Teller (BET) specific surface areas and pore volumes are summarized in Table 1. The MgO-Cs show increasing surface areas with decreasing average pore sizes because their micropore volumes, which have a large contribution to surface areas, increase with decreasing average pore sizes (Figure S1).

Table 1. BET Specific Surface Areas (BET SSAs) and Pore Volumes of MgO-Cs

samples	BET SSA[a] (m^2 g^{-1})	V_{total}[b] (cm^3 g^{-1})	V_{micro}[c] (cm^3 g^{-1})	V_{meso}[d] (cm^3 g^{-1})
MgO-C (5)	1530	1.81	0.55	1.26
MgO-C (10)	1100	1.95	0.41	1.54
MgO-C (30)	630	1.67	0.24	1.43

[a]Calculated using the adsorption isotherm at P/P_0 = 0.05−0.20. [b]Calculated from the adsorption amount of N_2 at P/P_0 = 0.96. [c]Calculated by the Dubinin−Radushkevich method. [d]Calculated by the equation: $V_{meso} = V_{total} - V_{micro}$.

We have previously reported that pyrene (PY) was adsorbed in both micropores and mesopores, irrespective of the amount of PY.[28] Therefore, all MgO-Cs can adsorb a large amount of PY due to their large total pore volumes.

PY was adsorbed on MgO-C in the gas phase, and the MgO-C/PY samples are denoted MgO-C (X)/PY (Y), where X and Y represent the average pore size of MgO-C and the weight percent of PY in the samples, respectively. The weight percentages of PY in the samples are 30 and 50 wt % because a large amount of PY incurs decreases in the utilization ratio of PY and the rate capability (*vide infra*), which were observed in our previous study using the activated carbon with the pore sizes of ∼4 nm.[24] Since the amount of the adsorbed PY is less than the saturation amount of MgO-Cs, there are few PY molecules on the particle surface of MgO-Cs, which were confirmed by the structural characterization and density measurement (for details, see Section S4 in the Supporting Information). Figure 1a shows the voltammograms of MgO-C (10)/PY (50) for the homocoupling of PY. CV was performed at 5 mV s^{-1} in a potential range of −0.1 to 1.2 V (*vs* Ag/AgCl) using an aqueous 1 M H_2SO_4 electrolyte. The potential window is rather wide for aqueous electrolytes because PY is not oxidized in 1 M H_2SO_4 below 0.9 V (*vs* Ag/AgCl),[24] which was confirmed from the voltammograms of the MgO-C/PY samples collected between −0.1 and 0.8 V (Figure S4). As shown in the figure, irreversible large anodic current is observed above 0.9 V at the first cycle, and subsequently, a cathodic peak emerges between 0.1 and 0.6 V in the reversed scan. This cathodic peak is paired with the anodic peak observed in the following cycle, indicating that PY was converted to a redox-active material. The peak current of the redox couple slightly increases, which is associated with the peak broadening (Figure 1a, inset), with increasing the cycle number. Meanwhile, the irreversible anodic current gradually decreases with increasing the cycle number. This is the typical voltammogram of the homocoupling of PY in the pores of all the MgO-Cs. The irreversible anodic current is attributed to the electrochemical oxidation of PY, while the reversible peak current is derived from the reversible redox reaction of PYD. CV was repeated until the voltammogram did not show any increase and decrease in the reversible and irreversible current, respectively. The homocoupling using CV has an advantage to visualize the progress of the homocoupling. The samples after the homocoupling are denoted MgO-C (X)/PYD (Y).

The formation of PYD was confirmed by MALDI-TOF-MS analysis. PYD was extracted by dichloromethane, and the extract was analyzed by MALDI-TOF-MS (see Section S5 for additional details). Figure 1b shows the MALDI-TOF-MS spectra of PY, PTFE, MgO-C (5)/PYD (30), and MgO-C (30)/PYD (50). PTFE was used to prepare the electrode and was not dissolved in dichloromethane. Therefore, the supernatant was analyzed and showed a peak at m/z of 234, probably derived from impurity. PY shows a peak at m/z of 202 corresponding to the molecular weight of PY. Meanwhile, MgO-C (5)/PYD (30) and MgO-C (30)/PYD (50) show a peak at m/z of 402 corresponding to the molecular weight of PYD. PY is known to be oxidized *via* electrochemical and photoionization methods,[25,28] and the resulting radical cation is unstable in comparison with those of larger aromatic hydrocarbons than PY due to the small charge delocalization region.[28] The formation mechanism of PYD is considered to be the same as the initial stage of the polymer formation, *i.e.*, electrochemical oxidation.[25] Radical cations should repel each

https://doi.org/10.1021/acsomega.2c04511
ACS Omega 2022, 7, 35245−35255

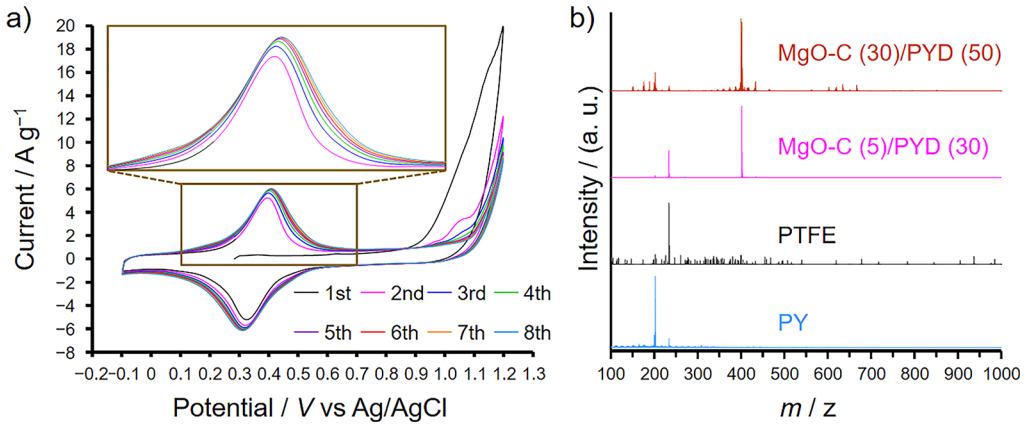

Figure 1. (a) Voltammograms of homocoupling for MgO-C (10)/PY (50) using an aqueous 1 M H_2SO_4 electrolyte performed at 5 mV s^{-1} in a potential range of −0.1 to 1.2 V (*vs* Ag/AgCl). (b) MALDI-TOF-MS spectra of PY, PTFE, MgO-C (5)/PYD (30), and MgO-C (30)/PYD (50).

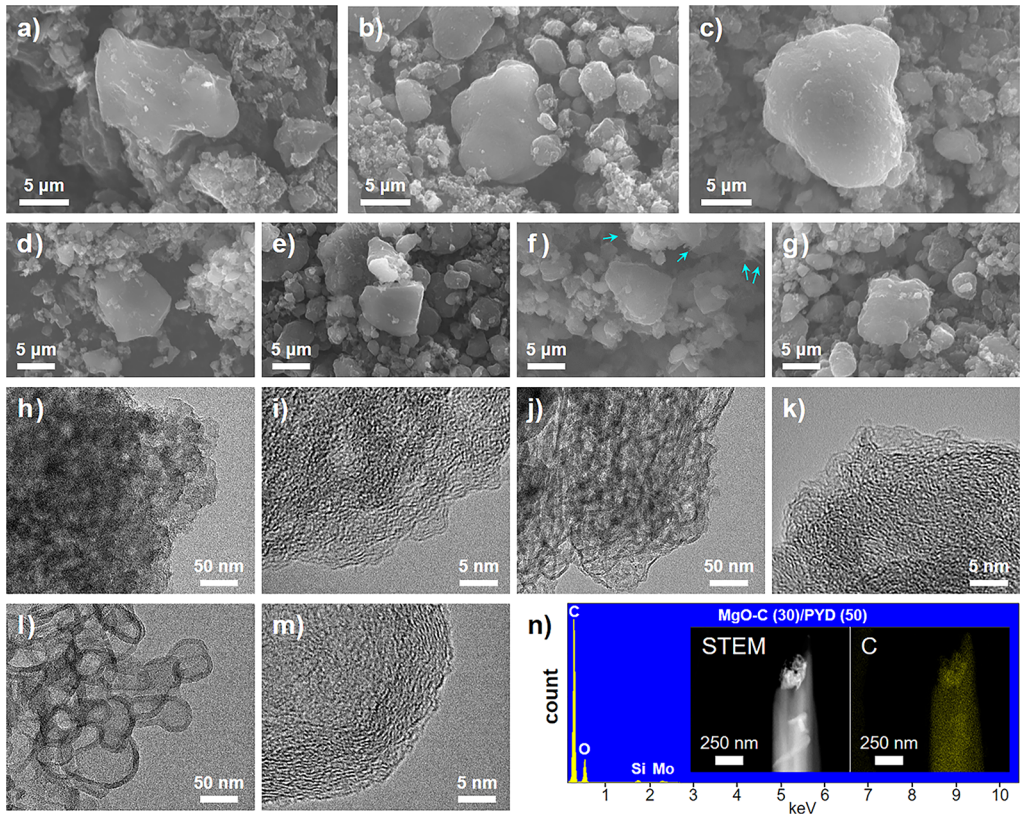

Figure 2. (a–g) SEM images of the electrodes of (a) MgO-C (5), (b) MgO-C (10), (c), MgO-C (30), (d) MgO-C (5)/PYD (50), (e) MgO-C (10)/PYD (50), (f) MgO-C (30)/PYD (50), and (g) MgO-C (30)/PYD (30). (h–m) TEM images of the electrodes of (h,i) MgO-C (5)/PYD (50), (j,k) MgO-C (10)/PYD (50), and (l,m) MgO-C (30)/PYD (50). (n) The EDS spectrum of the needle-shaped particles in MgO-C (30)/PYD (50). The inset shows the scanning transmission electron microscopy (STEM) image and the EDS mapping of carbon for the needle-shaped particle. All electrodes contain CB and PTFE.

other, but the formation of PYD upon polarization indicates that constrained pores enable the homocoupling of PY *via* radical cation intermediates, leaving two protons from ipso carbon atoms. The pore confinement would suppress further elongation of the PY unit. As shown in Figure 1a, many of the PY molecules would be dimerized at the first cycle and the remaining PY molecules gradually dimerized at the following cycles, which can be confirmed as a gradual increase in the current at the redox peak maxima and peak broadening.

PYD has redox-active characteristics and undergoes the reversible redox reaction inside the pores of MgO-C. This was validated by synthesizing PYD *via* the Suzuki–Miyaura homocoupling of 1-pyreneboronic acid using a Pd catalyst[29] and hybridizing PYD with MgO-C (5). The Suzuki–Miyaura homocoupling used in this study was the most simplified method among the reported methods to synthesize PYD but requires 1-pyreneboronic acid, $Pd(PPh_3)_4$, Na_2CO_3, and organic solvents. After the reaction, PYD must be removed from the solvent and purified through several processes. Moreover, PYD cannot be hybridized in the gas phase because PYD has a large molecular weight and does not readily vaporize. PYD was therefore adsorbed on MgO-C (5) through

https://doi.org/10.1021/acsomega.2c04511
ACS Omega 2022, 7, 35245−35255

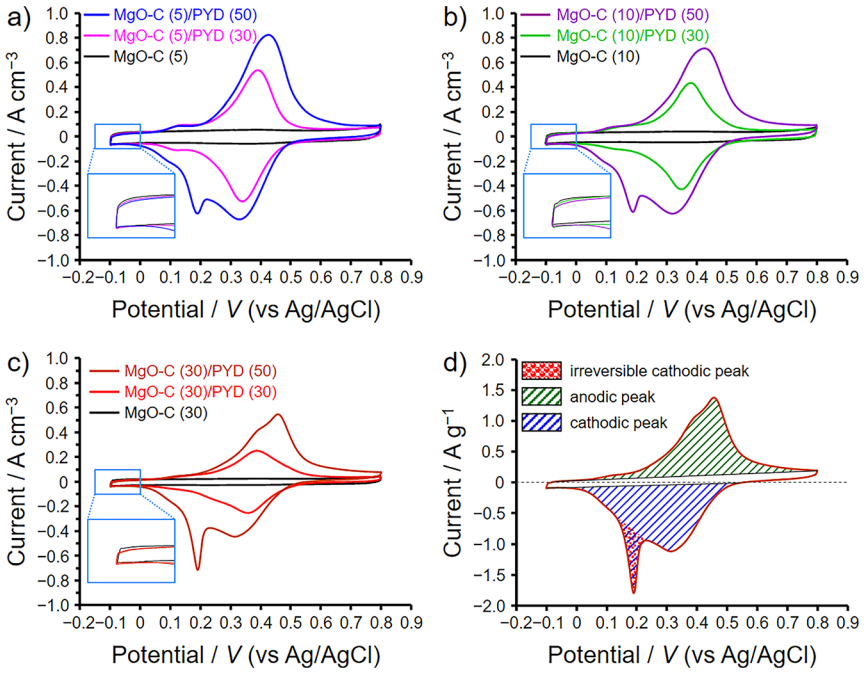

Figure 3. Cyclic voltammograms of the MgO-C/PYD hybrids collected at 1 mV s^{-1} in a potential range of −0.1 to 0.8 V. The results of the pristine MgO-Cs are plotted together. (a−c) Voltammograms of the hybrids for (a) MgO-C (5), (b) MgO-C (10), and (c) MgO-C (30). (d) Calculation of the quantity of currents derived from anodic and cathodic peaks and an irreversible cathodic peak. The insets show the magnified voltammogram between −0.15 and 0 V in a current range from −0.1 to 0.1 A cm^{-3}.

liquid-phase adsorption. In the liquid-phase adsorption, MgO-C (5) and PYD were mixed together at a MgO-C (5)/PYD weight ratio of 7:3, which is the same as the weight ratio of MgO-C (5) and PY in MgO-C (5)/PY (30). The mixture was stirred in dichloromethane for 24 h, followed by evaporation of the solvent (for details, see Section S8 in the Supporting Information). However, not all PYD was adsorbed inside the pores of MgO-C (5) in the resulting hybrid, MgO-C (5)/PYD (30)-L (Figure S8a). The voltammogram of MgO-C (5)/PYD (30)-L shows the same redox behavior as that of MgO-C (5)/PYD (30) (Figure S8b). On the other hand, the present hybridization method can use PY and does not need any metal catalysts, organic solvents, or purification processes, which is advantageous in terms of the feasibility and sustainable development in the application to the electrode preparation.

Figure 2a−g shows the SEM images of the electrodes of the pristine MgO-Cs and the MgO-C/PYD hybrids, which contain CB and binder (*i.e.*, PTFE). As shown in Figure 2a−c, all the MgO-Cs show polydispersity of the particle sizes. The primary particle sizes of the MgO-Cs (Figure S2) are much smaller than those of the particles in the SEM images, and the particles in Figure 2a−c are the secondary ones. By comparing with the SEM images of the pristine MgO-Cs, MgO-C (5)/PYD (50) and MgO-C (10)/PYD (50) do not show any difference in the morphology of the MgO-C particles, irrespective of a high PYD content (Figure 2d,e). On the other hand, MgO-C (30)/PYD (50) contains some needle-shaped particles, as indicated by arrows in the SEM image (Figure 2f). Since the needle-shaped particles were not confirmed by the SEM observations of any pristine MgO-Cs (Figure 2a−c), they are considered to be PYD deposited outside the MgO-C particles. Probably, the repulsion between radical cations surpassed the homocoupling of PY inside the large mesopores, leading to the desorption of radical cations, because PY forms large agglomerates inside the mesopores of MgO-C (30) (Figure S3). However, the stabilization of radical cations with counter anions (*i.e.*, SO_4^{2-}) and solvent molecules outside the mesopores would have led to the formation of PYD on the particle surface of MgO-C (30). The careful SEM observation of MgO-C (30)/PYD (50) confirmed that the amount of the needle-shaped PYD is not so large as to increase the electrode volume. We then conducted the SEM observation of MgO-C (30)/PYD (30), and no needle-shaped particles were observed in the samples (Figure 2g). Therefore, with the exception of MgO-C (30)/PYD (50), the hybridized PYD exists inside the pores of the MgO-Cs and therefore has a large contact area with conductive carbon surfaces. This is important to balance the volumetric capacitance enhancement and high power density as electrochemical capacitor electrodes. Figure 2h−m shows the TEM images of MgO-C (5)/PYD (50), MgO-C (10)/PYD (50), and MgO-C (30)/PYD (50) hybrids. By comparing with the TEM images of the pristine MgO-Cs (Figure S2), a difference in the structure of MgO-C particles is not observed in the TEM images between the pristine MgO-Cs and the MgO-C/PYD hybrids and any crystalline particles are not observed, suggesting that PYD did not form the crystalline structure inside the pores of MgO-Cs. The amorphous structure of PYD was confirmed from the XRD patterns of the MgO-C/PYD hybrids, which do not show distinct peaks derived from PY or PYD (Figure S6). The needle-like particles were analyzed by EDS, as shown in Figure 2n. The main component of the needle-shaped particle was carbon, but oxygen, silicone, and molybdenum were detected in the EDS spectrum. However, they were also detected in the EDS spectrum of a molybdenum grid used for the TEM observation (Figure S7c), and these elements are derived from the molybdenum grid. Moreover, an X-ray photoelectron spectroscopy analysis of the PY used in this study did not detect silicone and molybdenum (Figure S7a,b); the needle-shaped

https://doi.org/10.1021/acsomega.2c04511
ACS Omega 2022, 7, 35245−35255

particles are not derived from metal impurities in PY but are derived from PYD.

All electrochemical measurements of the MgO-C/PYD hybrids were performed without electrolyte exchange or electrode purification after the electrochemical oxidation (Figure 1a). Figure 3 shows the results of CV performed after the electrochemical oxidation. Note that the conditions of CV in Figure 1 are a wider potential range and a faster sweep rate than those in Figure 3 to dimerize PY and optimize the electrochemical capacitor behavior. On the other hand, the voltammograms in Figure 3a−c were collected at 1 mV s^{-1} in a potential range of −0.1 to 0.8 V to study the electrochemical behaviors of the MgO-C/PYD hybrids. The vertical axes in Figure 3a−c correspond to the volumetric current because the volume of MgO-C particles did not expand upon the adsorption of PY (Table S2) and the morphology of MgO-C particles did not change after the electrochemical oxidation (Figure 2). The voltammograms of all pristine MgO-Cs are characterized by a rectangular shape, typical of the EDL behavior of porous carbons. Meanwhile, the MgO-C/PYD hybrids show distinct anodic and cathodic peaks in their voltammograms. The distinct peak in the voltammogram suggests that a large contact area between PYD and conductive carbon surfaces facilitates rapid charge transfer at the contact interface. The voltammograms of the hybrids are characteristics of those of battery electrodes,[30] but the hybrids are used as electrochemical capacitor electrodes because the hybrids show the comparable to or higher charging and discharging characteristics than those of the corresponding pristine MgO-Cs (*vide infra*), which are used as EDLC electrodes,[26] and their rate capabilities are not balanced with those of battery electrodes. The volumetric current between −0.1 and 0 V is based on the EDL formation, while that between 0 and 0.8 V, where the anodic and cathodic peaks are observed, is derived from both the EDL formation and the redox reaction of PYD. The EDL-derived currents of the MgO-C/PYD hybrids are almost the same as those of the corresponding pristine MgO-Cs, as shown in the insets of the voltammograms. This result indicates that the impregnation of the electrolyte solution was not disturbed by the hybridized PYD and the remaining pores of the hybrids were almost fully filled with the electrolyte solution. Meanwhile, the EDL-derived current of the MgO-C/PY samples is much lower than that of the MgO-C/PYD hybrids due to the inadequacy of the electrolyte impregnation (Figure S4). The reason for the increase in the EDL-derived current after the electrochemical oxidation is due to the accelerated impregnation of the electrolyte solution by the high electric field, which is often observed in the voltammograms after the electrochemical oxidation.[23,24,31] The homocoupling of PY was performed by the electrochemical oxidation, and the potential range of the oxidation was between −0.1 and 1.2 V, which is wider than the potential range of CV in Figure 3 and Figure S4. At the high potential of ∼1.2 V, ions were strongly attracted by the high electric field, accelerating the impregnation of the electrolyte solution into the remaining pores of the MgO-C/PY samples. Therefore, the redox reaction of PYD would not be disturbed by the inadequacy of the electrolyte impregnation.

MgO-C (5)/PYD (50), MgO-C (10)/PYD (50), and MgO-C (30)/PYD (50) show a particularly distinct irreversible cathodic peak at 0.2 V, and this peak is not observed for the hybrids with a low PYD content. This peak is not attributed to the PYD formed outside the MgO-C particles because the needle-shaped PYD was observed only in MgO-C (30)/PYD (50). We thus calculated the quantity of electricity in the anodic and cathodic peaks by integrating the peak currents (Figure 3d) and compared the ratio of PY contributing to the capacitance enhancement to all the adsorbed PY (*i.e.*, the utilization ratio of PY). Based on the one-electron redox reaction per unit PY molecule in PYD, the calculated quantity of electricity exceeded the theoretical value, which was calculated from the total amount of PY adsorbed on MgO-Cs. Therefore, we supposed the two-electron redox reaction per unit PY molecule, and these results are summarized in Table 2. As shown in the table, the utilization ratio of PY

Table 2. Utilization Ratios of PY Calculated from Anodic and Cathodic Peak Current

	PY/30 wt %[a]		PY/50 wt %[a]	
	anodic	cathodic	anodic	cathodic[b]
MgO-C (5)	86	92	69	80 (4)
MgO-C (10)	74	76	60	79 (4)
MgO-C (30)	56	63	53	68 (7)
AC[c]	85	86	76	76[d]

[a]Weight percentage of PY in the MgO-C/PY or AC/PY samples. [b]The values in the parentheses are calculated from the irreversible cathodic peak. [c]The pore sizes of AC are less than 4 nm.[24] [d]No irreversible cathodic peak.

decreases with increasing both average pore sizes of MgO-Cs and the PY content. The utilization ratios of PY calculated from the cathodic peaks are, however, higher than those calculated from the anodic peaks for all MgO-C/PYD hybrids, and the difference is significant for the hybrids with a high PY content. We further calculated the quantity of current for the irreversible cathodic peak, as shown in Figure 3d, and the results are provided as the ratio to all the adsorbed PY (in a parenthesis in Table 2). However, the quantity of current for the irreversible cathodic peak is very small, and the difference between the utilization ratios calculated from the anodic and cathodic peaks cannot be explained only by the irreversible cathodic peak.

In our previous study, we used AC having both micropores and mesopores with the sizes of up to 4 nm, and the PY adsorbed inside the pores of the AC was subject to polarization under the same conditions used in this study.[24] But we did not calculate the utilization ratio of PY in the study. The weight percentage of PY in the AC/PY samples ranged from 10% to the saturation amount (*i.e.*, 60.2%), and all the samples after the electrochemical oxidation did not show any irreversible cathodic peaks. We then calculated the utilization ratios of PY for AC/PY (30%) and AC/PY (50%) after the electrochemical oxidation, and the results are added in Table 2. Clearly, there is little difference in the utilization ratios calculated from the anodic and cathodic peaks for these two hybrids. It is unknown what is attributed to the irreversible cathodic peak in the voltammograms, but we presume that some of the irreversible current may be derived from the desorption of the counter anions that were incorporated during the homocoupling as a redox impurity.[32] PY originally formed agglomerates consisting of multiple PY molecules and was oxidized at a high potential above 0.9 V (*vs* Ag/AgCl), resulting in the formation of PYD agglomerates inside the pores of MgO-Cs. At such a high potential, a large amount of anions must be diffused into the pores of MgO-Cs. The size of the PYD agglomerates in the

https://doi.org/10.1021/acsomega.2c04511
ACS Omega 2022, 7, 35245−35255

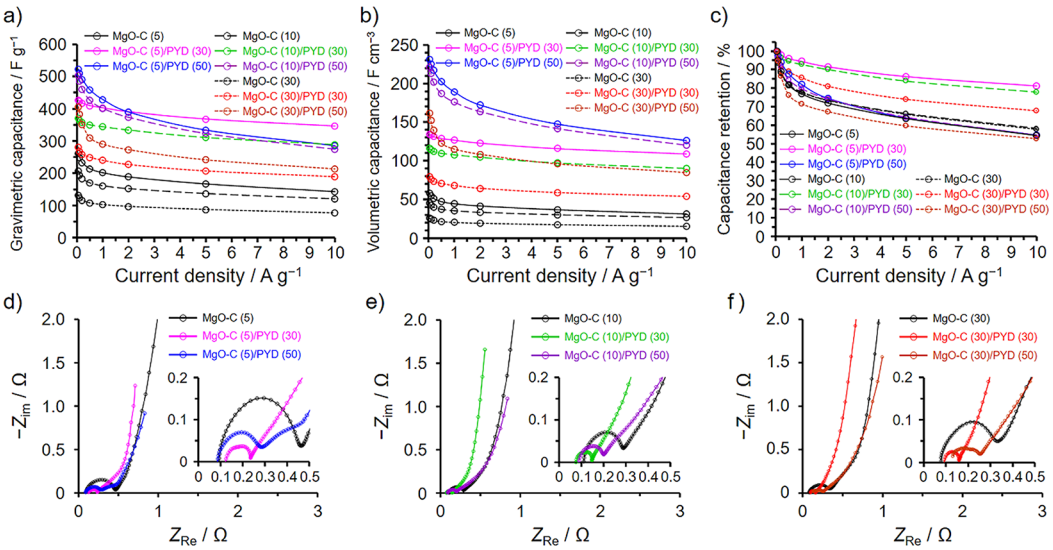

Figure 4. Results of electrochemical measurements for the MgO-C/PYD hybrids. The results of the pristine MgO-Cs are plotted together. (a,b) Dependence of (a) gravimetric capacitances and (b) volumetric capacitances on the current density. (c) Capacitance retentions based on the capacitances at 0.05 A g^{-1}. (d–f) Nyquist plots collected at the anodic peak top potential in Figure 3 for the hybrids of (d) MgO-C (5), (e) MgO-C (10), and (f) MgO-C (30). The Nyquist plots of the pristine MgO-Cs were collected at 0.5 V.

Table 3. Gravimetric and Volumetric Capacitances at 0.05 A g^{-1} and Capacitance Retentions at 0.05 A g^{-1} Based on the Capacitances at 10 A g^{-1} for the MgO-Cs and the MgO-C/PYD Hybrids

	MgO-C (5)			MgO-C (10)			MgO-C (30)		
PY (wt %)	F g^{-1}[a]	F cm^{-3}[a]	%[b]	F g^{-1}[a]	F cm^{-3}[a]	%[b]	F g^{-1}[a]	F cm^{-3}[a]	%[b]
0[c]	262	58	54	207	45	58	132	26	58
30	427 (165)	135 (77)	81	371 (164)	116 (71)	78	281 (149)	80 (54)	68
50	523 (261)	231 (173)	55	504 (297)	221 (176)	55	406 (274)	161 (135)	53

[a]The value in the parenthesis is the difference in the capacitance between the MgO-C/PYD hybrid and the corresponding pristine MgO-C. [b]Capacitance retention at 10 A g^{-1} based on the capacitance at 0.05 A g^{-1}. [c]The values in the line correspond to the results of the pristine MgO-Cs.

hybrids with a large amount of PY and/or a large average pore size is considered to be so large as to incorporate the anions. The fact that the current of the irreversible cathodic peak gradually decreased during electrochemical measurements suggests that the incorporated anions were gradually desorbed from the PYD agglomerates, especially at a low potential of ∼−0.1 V. The difference in the utilization ratio between the hybrids of AC and MgO-C (5) can be explained by the wide pore size distribution of MgO-Cs (Figure S1); the AC does not have the mesopores larger than 4 nm, and the size of PYD agglomerates was therefore restricted below 4 nm.

Figure 4a–c shows the results of the galvanostatic charge/discharge (GC) analysis. The capacitance was calculated from the GC curve of −0.1 to 0.8 V to exclude the effect of the irreversible cathodic current. Figure 4a,b shows the dependences of the gravimetric and volumetric capacitances on the current density, respectively. The gravimetric and volumetric capacitances at 0.05 A g^{-1} are summarized in Table 3. In addition, the capacitance retentions based on the capacitances at 0.05 A g^{-1} are plotted in Figure 4c, and the capacitance retentions at 10 A g^{-1} are added in Table 3. Note that the capacitance retentions calculated from the gravimetric and volumetric capacitances become the same value. The gravimetric capacitances of the pristine MgO-Cs at 0.05 A g^{-1} proportionally increase with their BET surface areas, and they show good capacitance retentions (54–58%) due to the reduced ion diffusion resistance by mesopores.[33,34] As shown in Figure 4a,b, the dependences of the gravimetric and volumetric capacitance enhancements on the amount of the hybridized PYD are clearly different. By comparing with the results of the pristine MgO-Cs, the volumetric capacitances of MgO-C (5)/PYD (30), MgO-C (10)/PYD (30), and MgO-C (30)/PYD (30) show more than a twofold increase (Figure 4b), and their capacitance retentions are enhanced more than 68% (Figure 4c). Since redox-active PYD was introduced inside the pores of MgO-C without the volume expansion of the MgO-C particles, the volumetric capacitance is enhanced by the hybridization of PYD. A further introduction of PYD is effective for further enhancing the volumetric capacitance, delivering a fourfold to sixfold increase in comparison with those of the pristine MgO-Cs over the whole current density region. The capacitance retentions consequently decrease to ∼53% but are still comparable to those of the pristine MgO-Cs; *i.e.*, the MgO-C/PYD hybrids can be used as electrochemical capacitor electrodes balancing the enhanced volumetric capacitance and high capacitance retention. These results promise a feasibility of the present hybridization of porous carbons with PYD toward high-performance electrochemical capacitor electrodes. As was confirmed in the SEM image, MgO-C (30)/PYD (50) contains the needle-shaped PYD on the particle surface of MgO-C. But the effect of the needle-shaped PYD on the electrochemical capacitor performance is negligible because the amount of the needle-shaped PYD is not large (Figure 2f). A relatively low volumetric capacitance enhancement by hybridizing with PYD is observed for the hybrids of MgO-C (30), which is ascribed to their low

https://doi.org/10.1021/acsomega.2c04511
ACS Omega 2022, 7, 35245−35255

utilization ratios of PY (Table 2). Meanwhile, the decrease in the capacitance retention for the hybrids with a high PYD content can be explained by the increase in the resistances of charge transfer and ion diffusion necessary for the redox reaction of PYD inside the PYD-constrained pores (*vide infra*).

The resistance components are comprised of the diffusion resistance (R_{diff}), the charge transfer resistance (R_{ct}), the bulk solution resistance (R_s), and the interfacial resistances between the MgO-C particles and between the current collector and the MgO-C particles (R_i).[35−37] Although the interfacial resistances between the MgO-C particles depends on the particle size of MgO-C, the resistance components of R_s and R_i can be considered to be almost the same values as far as the same MgO-C is used because all the electrodes were prepared under the precisely controlled conditions (for details, see the Experimental Section).[24,38] On the other hand, R_{diff} and R_{ct} are influenced by the amount of PYD and the average pore size of MgO-C. Figure 4d−f shows the Nyquist plots of the MgO-Cs and the MgO-C/PYD hybrids, which were collected at the anodic peak top potential. The semicircles in the high-frequency region corresponds to R_{ct},[39,40] and the locus in the low-frequency region is influenced by R_{diff}.[41] Despite the substantial charge transfer of PYD, all the hybrids exhibit smaller semicircles than those of the corresponding pristine MgO-Cs. The semicircle of the pristine MgO-C is attributed to the oxygen-containing functional groups,[39] which are mainly formed during acid etching to remove a template MgO, whereas their contribution to the pseudocapacitance is small for their large charge transfer resistance. On the other hand, the hybridized PYD shows substantial contribution to the volumetric capacitance enhancement (Figure 4b). However, the fact that the sizes of the semicircles of all the MgO-C/PYD hybrids are smaller than those of the corresponding pristine MgO-Cs indicates that the charge transfer between the conductive carbon surface and PYD is facilitated by the large contact area. In addition, ion diffusion is not disturbed for the hybrids with a moderate amount of PYD, which is confirmed from the locus in the low-frequency region with displaying almost a vertical line.[42] The decrease of R_{ct} is ascribed to the displacement of the charge transfer from the oxygen-containing functional groups to PYD, which can be also confirmed by comparing the Nyquist plots before and after the homocoupling of PY (Figure S5). These results suggest that the R_{ct} between the carbon surfaces and the hybridized PYD is lower than that of the oxygen-containing functional groups.

The fact that the capacitance retentions of MgO-C (5)/PYD (30), MgO-C (10)/PYD (30), and MgO-C (30)/PYD (30) are higher than those of the corresponding pristine MgO-Cs indicates that the redox reaction of the hybridized PYD proceeds faster than the EDL formation. It has been widely regarded that the EDL capacitance is superior to the pseudocapacitances in terms of the high power density. Since most of the redox-active materials have poor electrical conductivity, they are normally hybridized as micro- or nanosized structures such as particles and layers. Redox reactions of redox-active materials accompany the diffusion of electrons, but the diffusion distance of electrons for such large structures of redox-active materials must be longer than that of the PYD hybridized inside the pores of MgO-Cs. Therefore, the finely dispersed PYD inside the pores of MgO-Cs undergoes rapid charge transfer at the large contact interfaces. We have demonstrated the superior power densities of electrochemical capacitors than those of EDLCs using redox-active organic compounds[18,20−22] and redox-active organometallic complex,[23] which were hybridized inside the pores of porous carbons. That is, the redox reactions of redox-active materials are not intrinsically inferior to the EDL formation in terms of the power density. The key to obtain a high power density using redox-active materials lies in the way of hybridization, and our hybridization method can balance the enhancements of both high power density and high volumetric capacitance. A further introduction of PYD increases R_{diff} of MgO-C (5)/PYD (50), MgO-C (10)/PYD (50), and MgO-C (30)/PYD (50), which is expressed as a deviation of the locus in the low-frequency region from a vertical line.[43] The resulting R_{ct} slightly increases but is still lower than those of the pristine MgO-Cs. This is explained by the enlargement of the PYD agglomerates inside the pores of MgO-Cs. A large PYD agglomerate has a long charge transfer distance from the inner part of the agglomerate to the conductive carbon surface. In addition, a large amount of PYD also disturbs the ion diffusion necessary for the redox reaction of the PYD inside the pores. Consequently, R_{ct} and R_{diff} of the hybrids with a high PYD content increase, and their capacitance retentions become comparable to those of the pristine MgO-Cs.[28] These phenomena are consistent with the hybrids of all the MgO-Cs, but the hybrids with a high PYD content still show higher volumetric capacitances than those of the hybrids with a low PYD content over the whole current density region. Although MgO-Cs themselves are used as EDLC electrodes,[26] the MgO-C/PYD hybrids also show the comparable or superior capacitance retentions to those of the MgO-Cs. Therefore, the capacitance retentions of the MgO-C/PYD hybrids cannot be balanced with those of battery electrodes, and the MgO-C/PYD hybrids are used as electrochemical capacitor electrodes by combining with appropriate counterpart electrodes with compatible power densities (*i.e.*, asymmetrical electrochemical capacitors). Recently, high power density electrodes hybridizing metal oxides[44,45] and conductive polymers[46,47] have been reported, and these hybrid electrodes can be counterpart electrodes for the MgO-C/PYD hybrids.

The cycle tests of MgO-C (5)/PYD (50), MgO-C (10)/PYD (50), and MgO-C (30)/PYD (50) were examined at 1 A g^{-1} with a cell voltage from 0 to 0.8 V using an asymmetrical two-electrode cell, where the MgO-C/PYD hybrid and the corresponding pristine MgO-C were used as a cathode and an anode, respectively. The mass of the anode was balanced, considering the gravimetric capacitance of the MgO-C/PYD hybrid (for details, see the Supporting Information). For comparison, the cycle tests of the pristine MgO-Cs were examined using a symmetrical two-electrode cell. As shown in Figure 5, the capacitance retentions of the pristine MgO-Cs are more than 97% after 1000 cycles, while MgO-C (5)/PYD (50), MgO-C (10)/PYD (50), and MgO-C (30)/PYD (50) show the capacitance retentions of more than 88% after 1000 cycles. The decreases in the capacitance retentions of the asymmetrical cells are not attributed to the structural degradation of MgO-C particles because the symmetrical cells of the pristine MgO-Cs do not show a significant decrease in the capacitance retention. In addition, the absence of the structural change of MgO-C particles was confirmed by SEM and TEM observations (Figure S9). Meanwhile, the voltammograms of all the cathodes collected after the cycle test showed a decrease in the peak top current (Figure S10); the decreases in the capacitance retentions are explained by the

https://doi.org/10.1021/acsomega.2c04511
ACS Omega 2022, 7, 35245−35255

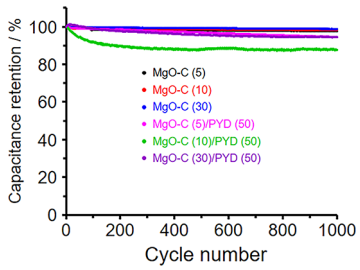

Figure 5. Results of the cycle test for MgO-C (5)/PYD (50), MgO-C (10)/PYD (50), and MgO-C (30)/PYD (50) collected at 1 A g^{-1} using an asymmetrical two-electrode cell. The results of the cycle tests for the pristine MgO-Cs measured using a symmetrical two-electrode cell are plotted together.

desorption of PYD from the pores of MgO-Cs during the cycle test.

The results obtained in this study reveal that the hybridization of PYD with the MgO-Cs enhances the volumetric capacitance with retaining the high capacitance retention and long cycle lifetimes. However, the utilization ratio of PY decreases with increasing both mesopore sizes and the amount of PY, resulting in a small volumetric capacitance enhancement. In our previous work, the AC with micropores and mesopores of ∼4 nm showed high utilization ratios of PY compatible with that of MgO-C (5) (Table 2), together with a high electrochemical capacitor performance. These results conclude that mesopores are effective to accommodate a large amount of PYD and balance the volumetric capacitance enhancement and high capacitance retention, whereas large mesopores decrease the utilization ratio of PY. In terms of the practical application of electrochemical capacitors, AC having not only micropores but also mesopores is an appropriate candidate for hybridizing PYD *via* the present method because AC is a low-cost porous carbon in comparison with other porous carbons. Moreover, most of ACs have micropores that effectively increase the surface area, and the electrode densities of AC are normally higher than those of MgO-Cs due to a large mesopore fraction of MgO-Cs,[52] which are advantageous to enhance the volumetric capacitance. The pore size of AC cannot be accurately controlled in a simple way, but AC does not normally have large mesopores like MgO-C (30).[48−50] Large mesopores are disadvantageous for effectively enhancing the volumetric capacitance, and the AC having not only micropores but also small mesopores is suitable for hybridizing PYD toward high-performance electrochemical capacitor electrodes. The superiority of our hybridization method is further emphasized by the absence of any metal catalysts, organic solvents, or the purification of the electrodes and solvent removal after the homocoupling.

4. CONCLUSIONS

In summary, we have demonstrated the homocoupling of PY into a dimer inside the pores of MgO-templated mesoporous carbons with the average pore sizes of 5, 10, and 30 nm through electrochemical oxidation without any metal catalysts or organic solvents. PYD was found to undergo reversible redox reaction and the redox reaction proceeded rapidly inside the pores due to a large contact area between PYD and conductive carbon surfaces. The hybridization was not associated with the volume expansion of mesoporous carbon particles, thereby enhancing the volumetric capacitance with retaining a high capacitance up to 10 A g^{-1}. The volumetric capacitance increased with increasing the amount of PY, but the utilization ratio of PY and the capacitance retention decreased with increasing the amount of PY. Therefore, considering the results of our previous work using the AC with the pore sizes of ∼4 nm, this study concludes that porous carbons with not only micropores but also small mesopores of *ca.* ∼5 nm are desirable for hybridizing PYD to balance high volumetric capacitance, high capacitance retention, and long cycle lifetimes. The resulting porous carbon/PYD hybrids can be used as high-performance electrochemical capacitor electrodes toward future electronic devices and others, by combining with suitable counterpart electrodes to balance their power densities. This hybridization can be applicable to commercial AC and is advantageous over other hybridization methods in terms of feasibility and waste minimization.

■ ASSOCIATED CONTENT

Supporting Information

The Supporting Information is available free of charge at https://pubs.acs.org/doi/10.1021/acsomega.2c04511.

Schemes S1 and S2. Schematic illustrations for electrode preparation and cell assembly. Figure S1. Nitrogen adsorption/desorption isotherms and pore size distributions of MgO-Cs. Figure S2. TEM images of MgO-Cs. Figure S3. XRD patterns of PY, MgO-Cs, and MgO-C/PY samples. Figure S4. Cyclic voltammograms of MgO-C/PY samples and MgO-C/PYD hybrids. Figure S5. Nyquist plots of MgO-C/PY samples and MgO-C/PYD hybrids. Figure S6. XRD patterns of the electrodes of MgO-C/PY samples and MgO-C/PYD hybrids. Figure S7. X-ray photoelectron spectra of PY and EDS spectrum. Figure S8. XRD pattern and cyclic voltammogram of MgO-C (5)/PYD (30)-L. Figure S9. SEM and TEM images of the cathodes after the cycle test. Figure S10. Voltammograms of the cathodes before and after the cycle test (PDF)

■ AUTHOR INFORMATION

Corresponding Author

Hiroyuki Itoi − *Department of Applied Chemistry, Faculty of Engineering, Aichi Institute of Technology, Toyota 470-0392, Japan;* orcid.org/0000-0002-1304-2707; Email: itoi-hiroyuki@aitech.ac.jp

Authors

Kazuki Takagi − *Department of Applied Chemistry, Faculty of Engineering, Aichi Institute of Technology, Toyota 470-0392, Japan*

Hayato Ohmi − *Department of Applied Chemistry, Faculty of Engineering, Aichi Institute of Technology, Toyota 470-0392, Japan*

Takanori Usami − *Department of Applied Chemistry, Faculty of Engineering, Aichi Institute of Technology, Toyota 470-0392, Japan*

Yuto Nagai − *Department of Applied Chemistry, Faculty of Engineering, Aichi Institute of Technology, Toyota 470-0392, Japan*

Chika Matsuoka − *Department of Applied Chemistry, Faculty of Engineering, Aichi Institute of Technology, Toyota 470-0392, Japan*

https://doi.org/10.1021/acsomega.2c04511
ACS Omega 2022, 7, 35245−35255

Ryutaro Suzuki − *Department of Applied Chemistry, Faculty of Engineering, Aichi Institute of Technology, Toyota 470-0392, Japan*
Shinichi Kugimiya − *Department of Applied Chemistry, Faculty of Engineering, Aichi Institute of Technology, Toyota 470-0392, Japan*
Hiroyuki Iwata − *Department of Electrical and Electronics Engineering, Aichi Institute of Technology, Toyota 470-0392, Japan*
Yoshimi Ohzawa − *Department of Applied Chemistry, Faculty of Engineering, Aichi Institute of Technology, Toyota 470-0392, Japan*

Complete contact information is available at: https://pubs.acs.org/10.1021/acsomega.2c04511

Notes

The authors declare no competing financial interest.

■ ACKNOWLEDGMENTS

This work was supported by JSPS KAKENHI grant no. 17K06034.

■ ABBREVIATIONS

AC, activated carbon; PY, pyrene; PYD, pyrene dimer; MgO-C, MgO-templated carbons; EDLC, electric double-layer capacitor

■ REFERENCES

(1) Pandolfo, A. G.; Hollenkamp, A. F. Carbon properties and their role in supercapacitors. *J. Power Sources* **2006**, *157*, 11−27.
(2) Frackowiak, E.; Béguin, F. Carbon materials for the electrochemical storage of energy in capacitors. *Carbon* **2001**, *39*, 937−950.
(3) Dong, H.; Yu, H.; Wang, X. Catalysis Kinetics and Porous Analysis of Rolling Activated Carbon-PTFE Air-Cathode in Microbial Fuel Cells. *Environ. Sci. Technol.* **2012**, *46*, 13009−13015.
(4) Deng, Q.; Li, X.; Zuo, J.; Ling, A.; Logan, B. E. Power generation using an activated carbon fiber felt cathode in an upflow microbial fuel cell. *J. Power Sources* **2010**, *195*, 1130−1135.
(5) Conway, B. E. *Electrochemical Supercapacitors, Scientific Fundamentals and Technological Applications*; Kluwer Academic/Plenum Press: New York, 1999.
(6) Song, Z.; Zhou, H. Towards sustainable and versatile energy storage devices: an overview of organic electrode materials. *Energy Environ. Sci.* **2013**, *6*, 2280−2301.
(7) Simon, P.; Gogotsi, Y. Materials for electrochemical capacitors. *Nat. Mater.* **2008**, *7*, 845−854.
(8) Aricò, A. S.; Bruce, P.; Scrosati, B.; Tarascon, J. M.; Van Schalkwijk, W. Nanostructured materials for advanced energy conversion and storage devices. *Nat. Mater.* **2005**, *4*, 366−377.
(9) Shao, Y.; El-Kady, M. F.; Sun, J.; Li, Y.; Zhang, Q.; Zhu, M.; Wang, H.; Dunn, B.; Kaner, R. B. Design and Mechanisms of Asymmetric Supercapacitors. *Chem. Rev.* **2018**, *118*, 9233−9280.
(10) Iwamura, S.; Fujita, K.; Iwashiro, R.; Mukai, S. R. Efficient preparation of TiO_2/C nanocomposite for electrode material through the liquid pulse injection technique. *Mater. Today Commun.* **2018**, *14*, 15−21.
(11) Donakowski, M. D.; Mansour, A. N.; Pala, I. R.; Chervin, C. N.; DeSario, P. A.; Long, J. W.; Rolison, D. R. Trapping a Ru_2O_3 Corundum-like Structure at Ultrathin, Disordered RuO_2 Nanoskins Expressed in 3D. *J. Phys. Chem. C* **2018**, *122*, 28895−28900.
(12) Lokhande, C. D.; Dubal, D. P.; Joo, O. S. Metal oxide thin film based supercapacitors. *Curr. Appl. Phys.* **2011**, *11*, 255−270.
(13) Chen, N.; Ren, Y.; Kong, P.; Tan, L.; Feng, H.; Luo, Y. In situ one-pot preparation of reduced graphene oxide/polyaniline composite for high-performance electrochemical capacitors. *Appl. Surf. Sci.* **2017**, *392*, 71−79.
(14) Wang, S.; Shang, J.; Wang, Q.; Zhang, W.; Wu, X.; Chen, J.; Zhang, W.; Qiu, S.; Wang, Y.; Wang, X. Enhanced Electrochemical Performance by Strongly Anchoring Highly Crystalline Polyaniline on Multiwalled Carbon Nanotubes. *ACS Appl. Mater. Interfaces* **2017**, *9*, 43939−43949.
(15) Shi, Y.; Yu, G. Designing Hierarchically Nanostructured Conductive Polymer Gels for Electrochemical Energy Storage and Conversion. *Chem. Mater.* **2016**, *28*, 2466−2477.
(16) Zhu, L.; Ding, G.; Xie, L.; Cao, X.; Liu, J.; Lei, X.; Ma, J. Conjugated Carbonyl Compounds as High-Performance Cathode Materials for Rechargeable Batteries. *Chem. Mater.* **2019**, *31*, 8582−8612.
(17) Suga, T.; Ohshiro, H.; Sugita, S.; Oyaizu, K.; Nishide, H. Emerging N-Type Redox-Active Radical Polymer for a Totally Organic Polymer-Based Rechargeable Battery. *Adv. Mater.* **2009**, *21*, 1627−1630.
(18) Itoi, H.; Yasue, Y.; Suda, K.; Katoh, S.; Hasegawa, H.; Hayashi, S.; Mitsuoka, M.; Iwata, H.; Ohzawa, Y. Solvent-free Preparation of Electrochemical Capacitor Electrodes Using Metal-free Redox Organic Compounds. *ACS Sustainable Chem. Eng.* **2017**, *5*, 556−562.
(19) Itoi, H. Enhancing the performance of electrochemical capacitor electrodes by modifying their carbon nanopores with redox-active materials. *Tanso* **2019**, *2019*, 103−113.
(20) Itoi, H.; Hasegawa, H.; Iwata, H.; Ohzawa, Y. Non-polymeric hybridization of a TEMPO derivative with activated carbon for high-energy-density aqueous electrochemical capacitor electrodes. *Sustainable Energy Fuels* **2018**, *2*, 558−565.
(21) Itoi, H.; Tazawa, S.; Hasegawa, H.; Tanabe, Y.; Iwata, H.; Ohzawa, Y. Study of the pore structure and size effects on the electrochemical capacitor behaviors of porous carbon/quinone derivative hybrids. *RSC Adv.* **2019**, *9*, 27602−27614.
(22) Itoi, H.; Kotani, S.; Tanabe, Y.; Kasai, Y.; Suzuki, R.; Miyaji, M.; Iwata, H.; Ohzawa, Y. Study of the mesopore size effect on the electrochemical capacitor behaviors of mesoporous carbon/quinone derivative hybrids. *Electrochim. Acta* **2020**, *362*, No. 137119.
(23) Itoi, H.; Ninomiya, T.; Hasegawa, H.; Maki, S.; Sakakibara, A.; Suzuki, R.; Kasai, Y.; Iwata, H.; Matsumura, D.; Ohwada, M.; Nishihara, H.; Ohzawa, Y. Unusual Redox Behavior of Ruthenocene Confined in the Micropores of Activated Carbon. *J. Phys. Chem. C* **2020**, *124*, 15205−15215.
(24) Itoi, H.; Maki, S.; Ninomiya, T.; Hasegawa, H.; Matsufusa, H.; Hayashi, S.; Iwata, H.; Ohzawa, Y. Electrochemical polymerization of pyrene and aniline exclusively inside the pores of activated carbon for high-performance asymmetric electrochemical capacitors. *Nanoscale* **2018**, *10*, 9760−9772.
(25) Bachman, J. C.; Kavian, R.; Graham, D. J.; Kim, D. Y.; Noda, S.; Nocera, D. G.; Shao-Horn, Y.; Lee, S. W. Electrochemical polymerization of pyrene derivatives on functionalized carbon nanotubes for pseudocapacitive electrodes. *Nat. Commun.* **2015**, *6*, 7040−7048.
(26) Kado, Y.; Imoto, K.; Soneda, Y.; Yoshizawa, N. Highly enhanced capacitance of MgO-templated mesoporous carbons in low temperature ionic liquids. *J. Power Sources* **2014**, *271*, 377−381.
(27) Morishita, T.; Tsumura, T.; Toyoda, M.; Przepiórski, J.; Morawski, A. W.; Konno, H.; Inagaki, M. A review of the control of pore structure in MgO-templated nanoporous carbons. *Carbon* **2010**, *48*, 2690−2707.
(28) Ohkubo, K.; Kohno, N.; Yamada, Y.; Fukuzumi, S. Metal-free hydrogen evolution with nanoparticles derived from pyrene via two-photon ionization induced by laser irradiation. *Chem. Commun.* **2015**, *51*, 11515−11518.
(29) Yuichi, K.; Atsushi, N.; Yoshiki, C. Microwave-assisted One-pot Synthesis of Luminescent Organic−Inorganic Hybrids via Simultaneous Process of Sol−Gel and Suzuki−Miyaura Coupling Reactions. *Chem. Lett.* **2010**, *39*, 480−481.
(30) Brousse, T.; Bélanger, D.; Long, J. W. To Be or Not To Be Pseudocapacitive? *J. Electrochem. Soc.* **2015**, *162*, A5185−A5189.
(31) Itoi, H.; Ito, M.; Kasai, Y.; Tanabe, Y.; Suzuki, R.; Hasegawa, H.; Miyaji, M.; Iwata, H.; Ohzawa, Y.; Beniya, A.; Higashi, S. Study of

the pore size effect on the charge storage of hydrous RuO_2 nanoparticles supported within the pores of activated carbon. *Solid State Sci.* **2021**, *111*, No. 106472.
(32) Wang, K.; Yao, L.; Jahon, M.; Liu, J.; Gonzalez, M.; Liu, P.; Leung, V.; Zhang, X.; Ng, T. N. Ion-Exchange Separators Suppressing Self-Discharge in Polymeric Supercapacitors. *ACS Energy Lett.* **2020**, *5*, 3276−3284.
(33) Jurewicz, K.; Vix-Guterl, C.; Frackowiak, E.; Saadallah, S.; Reda, M.; Parmentier, J.; Patarin, J.; Béguin, F. Capacitance properties of ordered porous carbon materials prepared by a templating procedure. *J. Phys. Chem. Solids* **2004**, *65*, 287−293.
(34) Xing, W.; Qiao, S. Z.; Ding, R. G.; Li, F.; Lu, G. Q.; Yan, Z. F.; Cheng, H. M. Superior electric double layer capacitors using ordered mesoporous carbons. *Carbon* **2006**, *44*, 216−224.
(35) Nian, Y.-R.; Teng, H. Nitric acid modification of activated carbon electrodes for improvement of electrochemical capacitance. *J. Electrochem. Soc.* **2002**, *149*, A1008−A1014.
(36) Wang, K.-P.; Teng, H. Structural Feature and Double-Layer Capacitive Performance of Porous Carbon Powder Derived from Polyacrylonitrile-Based Carbon Fiber. *J. Electrochem. Soc.* **2007**, *154*, A993−A998.
(37) Huang, C.-W.; Teng, H. Influence of Carbon Nanotube Grafting on the Impedance Behavior of Activated Carbon Capacitors. *J. Electrochem. Soc.* **2008**, *155*, A739−A744.
(38) Itoi, H.; Nishihara, H.; Kogure, T.; Kyotani, T. Three-Dimensionally Arrayed and Mutually Connected 1.2-nm Nanopores for High-Performance Electric Double Layer Capacitor. *J. Am. Chem. Soc.* **2011**, *133*, 1165−1167.
(39) Itoi, H.; Nishihara, H.; Ishii, T.; Nueangnoraj, K.; Berenguer-Betrián, R.; Kyotani, T. Large Pseudocapacitance in Quinone-Functionalized Zeolite-Templated Carbon. *Bull. Chem. Soc. Jpn.* **2014**, *87*, 250−257.
(40) Tong, J.; Zhang, H.; Gu, J.; Li, L.; Ma, C.; Zhao, J.; Wang, C. Poly(ethylene glycol)-block-poly(propylene glycol)-block-poly-(ethylene glycol)-assisted synthesis of graphene/polyaniline composites as high-performance supercapacitor electrodes. *J. Mater. Sci.* **2016**, *51*, 1966−1977.
(41) Wang, Y.; Shi, Z.; Huang, Y.; Ma, Y.; Wang, C.; Chen, M.; Chen, Y. Supercapacitor Devices Based on Graphene Materials. *J. Phys. Chem. C* **2009**, *113*, 13103−13107.
(42) Stoller, M. D.; Park, S.; Zhu, Y.; An, J.; Ruoff, R. S. Graphene-Based ultracapacitors. *Nano Lett.* **2008**, *8*, 3498−3502.
(43) Chen, W.-C.; Wen, T.-C.; Teng, H. Polyaniline-deposited porous carbon electrode for supercapacitor. *Electrochim. Acta* **2003**, *48*, 641−649.
(44) Ji, S.-H.; Chodankar, N. R.; Kim, D.-H. Aqueous asymmetric supercapacitor based on RuO_2-WO_3 electrodes. *Electrochim. Acta* **2019**, *325*, No. 134879.
(45) An, C.; Zhang, Y.; Guo, H.; Wang, Y. Metal oxide-based supercapacitors: progress and prospectives. *Nanoscale Adv.* **2019**, *1*, 4644−4658.
(46) Wang, L.; Li, X.; Wang, G. Construction of an electrochemical stable conductive network to improve the pseudocapacitance of polyaniline. *Electrochim. Acta* **2020**, *331*, No. 135279.
(47) Cui, M.; Wang, F.; Zhang, Z.; Min, S. Polyaniline-filled carbonized wood membrane as an advanced self-supported electrode for superior pseudocapacitive energy storage. *Electrochim. Acta* **2020**, *359*, No. 136961.
(48) Qu, D.; Shi, H. Studies of activated carbons used in double-layer capacitors. *J. Power Sources* **1998**, *74*, 99−107.
(49) Barbieri, O.; Hahn, M.; Herzog, A.; Kötz, R. Capacitance limits of high surface area activated carbons for double layer capacitors. *Carbon* **2005**, *43*, 1303−1310.
(50) Kierzek, K.; Frackowiak, E.; Lota, G.; Gryglewicz, G.; Machnikowski, J. Electrochemical capacitors based on highly porous carbons prepared by KOH activation. *Electrochim. Acta* **2004**, *49*, 515−523.

https://doi.org/10.1021/acsomega.2c04511
ACS Omega 2022, 7, 35245−35255